Journal of Energy Chemistry 65 (2022) 646–653

Contents lists available at ScienceDirect

Journal of Energy Chemistry

journal homepage: www.elsevier.com/locate/jechem

http://www.journals.elsevier.com/journal-of-energy-chemistry/

CO_2-adsorbent spongy electrode for non-aqueous Li–O_2 batteries

Yiseul Yoo [a,b], Giseung Lee [c], Min-Gi Jeong [a], Hun-Gi Jung [a], Sunghee Shin [a,d], Dongjin Byun [b], Taeeun Yim [c,*], Hee-Dae Lim [a,*]

[a] Center for Energy Storage Research, Korea Institute of Science and Technology (KIST), Hwarang-ro 14-gil 5, Seongbuk-gu, Seoul 02792, Republic of Korea
[b] Department of Materials Science and Engineering, Korea University, 145 Anam-ro, Seongbuk-gu, Seoul 02841, Republic of Korea
[c] Department of Chemistry, Incheon National University, 119 Academy-ro, Yeonsu-gu, Incheon 22012, Republic of Korea
[d] Department of Chemical and Biological Engineering, Korea University, Seoul 02841, Republic of Korea

ARTICLE INFO

Article history:
Received 24 March 2021
Revised 17 June 2021
Accepted 22 June 2021
Available online 15 July 2021

Keywords:
Li–O_2 battery
Benzylamine
CO_2 adsorption
Li_2CO_3
Li_2O_2
CO_2-sponging electrode

ABSTRACT

Regulation of the Li_2CO_3 byproduct is the most critical challenge in the field of non-aqueous Li–O_2 batteries. Although considerable efforts have been devoted to preventing Li_2CO_3 formation, no approaches have suggested the ultimate solution of utilizing the clean Li_2O_2 reaction instead of that of Li_2CO_3. Even if extremely pure O_2 is used in a Li–O_2 cell, its complete elimination is impossible, eventually generating CO_2 gas during charge. In this paper, we present the new concept of a CO_2-adsorbent spongy electrode (CASE), which is designed to trap the evolved CO_2 using adsorption materials. Various candidates composed of amine functional groups (–NH_2) for capturing CO_2 were screened, with quadrapurebenzylamine (QPBZA) exhibiting superior CO_2-adsorbing ability among the proposed candidates. Accordingly, we fabricated the CASE by sandwiching QPBZA between porous carbon layers, which facilitated the transport of gaseous products. The new electrode was demonstrated to effectively capture the evolved CO_2 during charge, therefore altering the reaction pathways to the ideal case. It is highly advantageous to mitigate the undesirable CO_2 incorporation in the next discharge, resulting in improved cyclability. This novel concept of a CO_2-sponging electrode provides an alternative route to the realization of practically meaningful Li–O_2 batteries.

1. Introduction

Li–air and Li–O_2 batteries have received considerable attention as potential high-energy–density energy storage devices that can far surpass the performance of current Li-ion batteries (LIBs). The attractive reaction between Li ions and oxygen in the absence of any intercalation host ($2Li^+ + O_2(g) + 2e^- \leftrightarrow Li_2O_2(s)$, E^0 = 2.96 V vs. Li/Li^+) enables the delivery of an extremely high theoretical energy density (~3500 Wh kg^{-1}), and the use of the environmentally friendly and unlimited source of oxygen holds great promise for next-generation LIBs [1,2]. Since the first introduction of a rechargeable Li–O_2 battery [3], substantial progress has been made, especially in the development of efficient cathode materials by using functionalized carbon (i.e., air cathodes) [4–6], which deliver extremely large discharge capacities far beyond those of current LIBs [7–10]. However, the practically important properties of coulombic efficiency and cyclability remain relatively inferior to those of LIBs. These limitations of Li–O_2 batteries mainly stem from side reactions, which lead to the accumulation of solid byproducts and markedly reduce cell performance [11].

Among the problematic byproducts, Li_2CO_3 is a leading contributor to cycle degradation and poor efficiency; this compound is prone to form and accumulate on the cathode surface, eventually resulting in premature cell death [12,13]. Unfortunately, the undesirable side reaction is difficult to prevent because it is easily triggered by various routes: (1) the incorporation reaction between residual CO_2 and O_2^- during discharge [14,15], (2) electrolyte decomposition at high voltages [12,16,17], and (3) spontaneous chemical reaction between Li_2O_2 and the carbon electrode [12,16,18,19]. Although considerable efforts have been made to alleviate the formation and accumulation of Li_2CO_3; thus far, no method offers a perfect solution that can simultaneously prevent all the routes. One creative solution that has been previously suggested is the use of a carbon-free electrode [20–22]. In the absence of reactive carbon, the use of a precious metal substrate was effective in preventing the formation of Li_2CO_3; nevertheless, the complete prevention of Li_2CO_3 formation was not possible. Alternatively, the use of solid and liquid catalysts for electrochem-

* Corresponding authors.
E-mail addresses: yte0102@inu.ac.kr (T. Yim), hdlim@kist.re.kr (H.-D. Lim).

https://doi.org/10.1016/j.jechem.2021.06.022

ical decomposition of Li_2CO_3 has been suggested [23,24]. Some effective catalysts have been proposed and demonstrated to decompose Li_2CO_3 by detecting CO_2 gas during charge. However, even if most of the Li_2CO_3 can be decomposed, the generated CO_2 would be easily reincorporated in the next discharge ($2CO_2 + 4Li^+ + O_2 + 4e^- \rightarrow 2Li_2CO_3$) [25]. The high gas solubility of CO_2 in an aprotic electrolyte compared with that of O_2 (approximately 50 times higher) may accelerate the incorporation reaction [26]. Recognizing that the evolution of CO_2 as well as the undesirable incorporation are indispensable in the Li–O_2 cell, a completely new approach to eliminate the evolved CO_2 in the cell is required for the advancement of practical Li–O_2 batteries.

In this paper, we for the first time suggest a new CO_2-adsorbent spongy electrode (CASE) composed of a porous carbon substrate decorated with CO_2-adsorption materials (CAMs) for practical Li–O_2 batteries. Our concept for regulating the CO_2 incorporation is to trap the evolved CO_2 using CAM materials. If the CO_2 can be stably captured, its subsequent reaction would be greatly regulated, thereby promoting the ideal Li_2O_2 circulation. Through various feasibility tests, the most suitable CAM of quadrapurebenzylamine (QPBZA) was selected owing to its superior CO_2-adsorption ability and high stability. By sandwiching the QPBZA particles between carbon layers, the porous CASE with unique features was fabricated. The electrode was demonstrated to effectively capture CO_2 during charge, which could alter the reaction route to the ideal case, resulting in improved cyclability.

2. Experimental

2.1. Characterization of CAMs

The six CAM candidates, DIPA, ODA, PZ, AP Sg, EDP Sg, and QPBZA, were purchased from Sigma Aldrich. The morphologies of the CAMs were analyzed using FE-SEM (Inspect F, FEI Corp.). For bonding analysis, XPS (Thermo Scientific) and FT-IR (PerkinElmer) were used. To define the surface area and pore size distribution, the BET (TriStar 3000, Micromeritics, USA) method was used based on the N_2 adsorption–desorption reaction at −195.8 °C. The thermal stability was evaluated using DSC (PerkinElmer) under N_2 atmosphere.

2.2. Preparation of CASE air electrode

Pristine QPBZA was grinded into T-QPBZA using an ultra-compact FRITSCH mini-mill with 90 oscillations per second for 2 h. Then, the T-QPBZA was thermally activated by vacuum drying at 100 °C. Next, 0.16 g of T-QPBZA and 0.14 g of MWCNTs (MR99, surface area 225.33 $m^2\ g^{-1}$, purity > 99 wt%, average diameter 10 nm) were dispersed in acetone and distilled water solution in a volume ratio of 1:4 via tip sonication (550 Sonic Dismembrator, Fisher Scientific) for 90 min. The mixture slurries were filtered and dried at 60 °C for 30 min to finally produce a binder-free and self-standing CASE.

2.3. Electrochemical tests and analyses

All the prepared CASEs were dried overnight at 100 °C under vacuum to remove moisture before cell assembly. Nickel foam, the prepared air electrode, a separator (GF/F, Whatman glass microfiber filters), and lithium metal were assembled in order in an Ar-filled glovebox (H_2O < 0.1 ppm, O_2 < 0.1 ppm), and the electrochemical performances were evaluated using R2032 coin-type cells (Wellcos Corp.), which had a hole (0.5 mm in diameter) at the center of the bottom as a gas pathway. 1 M lithium bis(trifluor omethanesulfonyl)amide (LiTFSI) in tetraethylene glycol dimethyl ether (TEGDME) was used as the liquid electrolyte (H_2O < 30 ppm). All the cells were relaxed for 2 h before performing the tests to ensure cell stabilization and were operated under a pure oxygen condition (purity N5.0) using a potentio-galvanostat cycler (WBCS3000S battery cycler, WonATech). To quantify the amount of evolved CO_2, differential electrochemical mass spectrometry (DEMS, HPR-20 R&D, Hiden Analytical) was performed. Electrochemical impedance spectroscopy (EIS) analysis was performed by using the VMP3 (Biologic potentio-galvanostat) instrument with frequency from 1 MHz to 10 mHz at 10 mV in series cycles.

3. Results and discussion

Fig. 1(a and b) schematically illustrate the different mechanisms describing the ideal and real cases of Li–O_2 cells, respectively. Supposing the ideal case where the discharge only proceeds by Li_2O_2 formation, the charge process will produce only clean O_2 (described as $^*O_2$ in the dotted box in Fig. 1a). Then, the clean O_2 can be reused in the next discharge, and the ideal Li_2O_2 formation and decomposition reactions will be continued. However, once the undesirable Li_2CO_3 is included in the real case of a Li–O_2 cell (Fig. 1b), it is impossible to fully eliminate Li_2CO_3, which gradually degrades the cell performance. Even if Li_2CO_3 can be partially decomposed at high voltages [27], the newly generated CO_2 ($^*CO_2$ in the dotted box in Fig. 1b) is prone to reincorporation in the next discharge process (i.e., the CO_2 incorporation).

The different reaction pathways can be experimentally verified by testing two cell types of opened and closed cells, as shown in Fig. 1(c and d). The opened cell is the generally used type, where highly pure O_2 (99.999%) is continuously injected into a cell under high pressure during a electrochemical test. As long as fresh O_2 is unlimitedly overflowed, undesirable gaseous species (e.g., the evolved $^*CO_2$) can be rapidly swept away. In contrast, the closed cell is an air-tight sealed system after the injection of sufficient O_2 into a cell; therefore, any evolved CO_2 ($^*CO_2$) cannot flow out because of the absence of an exit. The closed condition easily triggers the CO_2 incorporation during the next reduction process, leading to the regeneration of Li_2CO_3, as described in Fig. 1(b). Although the opened cell also produces the Li_2CO_3 byproduct to some degree, it is more analogous to the ideal case while the closed cell represents the real case. As shown in Fig. 1(c and d), the opened cell results in a higher energy efficiency with increased cyclability compared with the closed cell. These phenomena explain why most previous Li–O_2 cells have been operated in the opened cell system and why highly pure oxygen has been used instead of ambient air. Considering that the required volume of O_2 to theoretically deliver 1 mAh of Li_2O_2 reaction is only approximately 417.89 μL, Li–O_2 experiments in opened systems waste a lot of expensive pure O_2 gas. Unfortunately, the formation of Li_2CO_3 is unavoidable in current Li–O_2 technologies regardless of the cell systems, and the generation of CO_2 gas is also indispensable; therefore, a new approach to regulate $^*CO_2$ is needed for the realization of clean Li–O_2 batteries.

We suggested a capturing strategy using a CASE to effectively eliminate $^*CO_2$, as schematically described in Fig. 2(a). A sponge-like air electrode was designed by sandwiching micro-sized CAM particles between the carbon layers. The unique structure is expected to facilitate the fast transport of reaction products (O_2 and Li^+); at the same time, undesirable $^*CO_2$ could be captured by the CAM particles positioned in the gaps between carbon layers (image between discharged and charged CASE in Fig. 2a). Notably, the porous design of carbon substrate decorated with CAMs would be effective in maximizing the activity of CAM. If the $^*CO_2$ could be restricted and well trapped, the CASE might be able to prevent the incorporation of Li_2CO_3 as well as improve the electrochemical per-

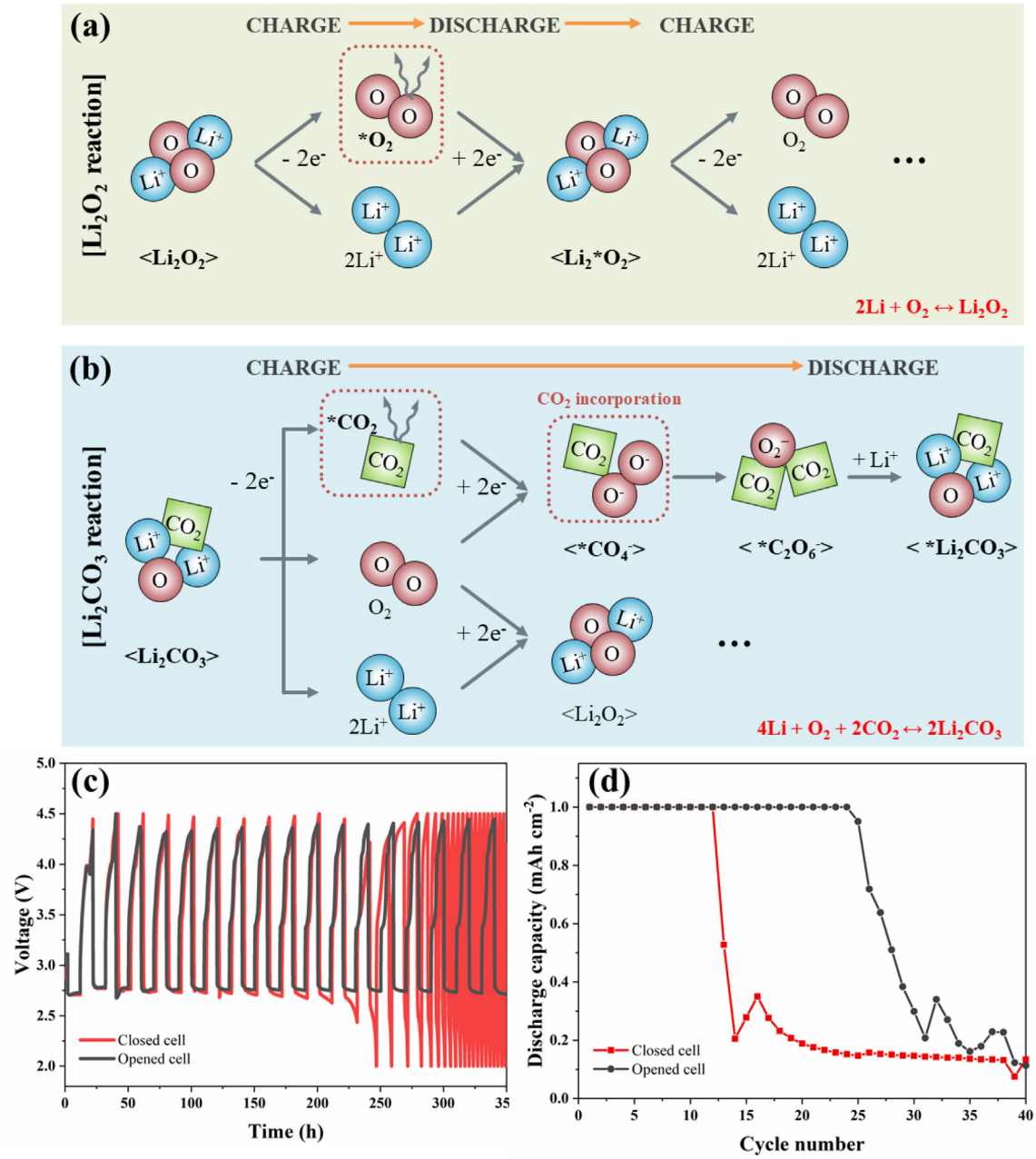

Fig. 1. Reaction mechanism for the formation and decomposition of (a) Li_2O_2 and (b) Li_2CO_3 discharge products for Li–O_2 cells. (c) Electrochemical discharge and charge profiles of Li–O_2 cells in the different operating systems of the opened and closed cells. (d) Comparison of cyclabilities for the two cell systems.

formance. In addition, for reuse, the CASE is designed to recover to the pristine state by detaching the entangled $*CO_2$ on CAM particles (image between charged and activated CASE in Fig. 2a) through a simple thermal treatment.

Finding an appropriate CAM is the first step in fabricating a CASE; therefore, we considered the essential requirements of an effective CAM. The ideal CAM should ideally (1) selectively adsorb CO_2 molecules, (2) have a high adsorption ability per unit mass, and (3) have a negligible solubility in the electrolyte. In addition, it should be (4) thermally and chemically stable in a Li–O_2 cell and (5) reusable through a thermal activation process (i.e., CO_2 desorption process). As amine functional groups have been known as an effective adsorbent for CO_2 [28,29], the amine-functionalized task-specific CAM candidates diisopropanolamine (DIPA), octadecylamine (ODA), piperazine (PZ), 3-aminopropyl-functionalized silica gel (AP Sg), 3-(ethylenediamino)propyl-functionalized silica gel (EDP Sg), and QPBZA were employed. SEM image of each candidate and the corresponding chemical information are presented in Fig. 2(b–g). Additionally, the expected reaction mechanism of each CAM with CO_2 is described in Fig. S1.

To determine the most suitable CAM among the candidates, their feasibilities were evaluated using various tests, as shown in Fig. 3. As the CAM operates when wet in the electrolyte to directly trap the soluble CO_2, the prior requirement would be a negligible solubility. If the CAM was soluble and detachable from the air cathode, the adsorption ability would be seriously decreased and might trigger unexpected side reactions. To verify the solubility, 0.1 g of each candidate was dispersed in 1 mL of the electrolyte and placed at room temperature for 1 day without mechanical stirring (Fig. 3a). DIPA and PZ were partially soluble in the electrolyte;

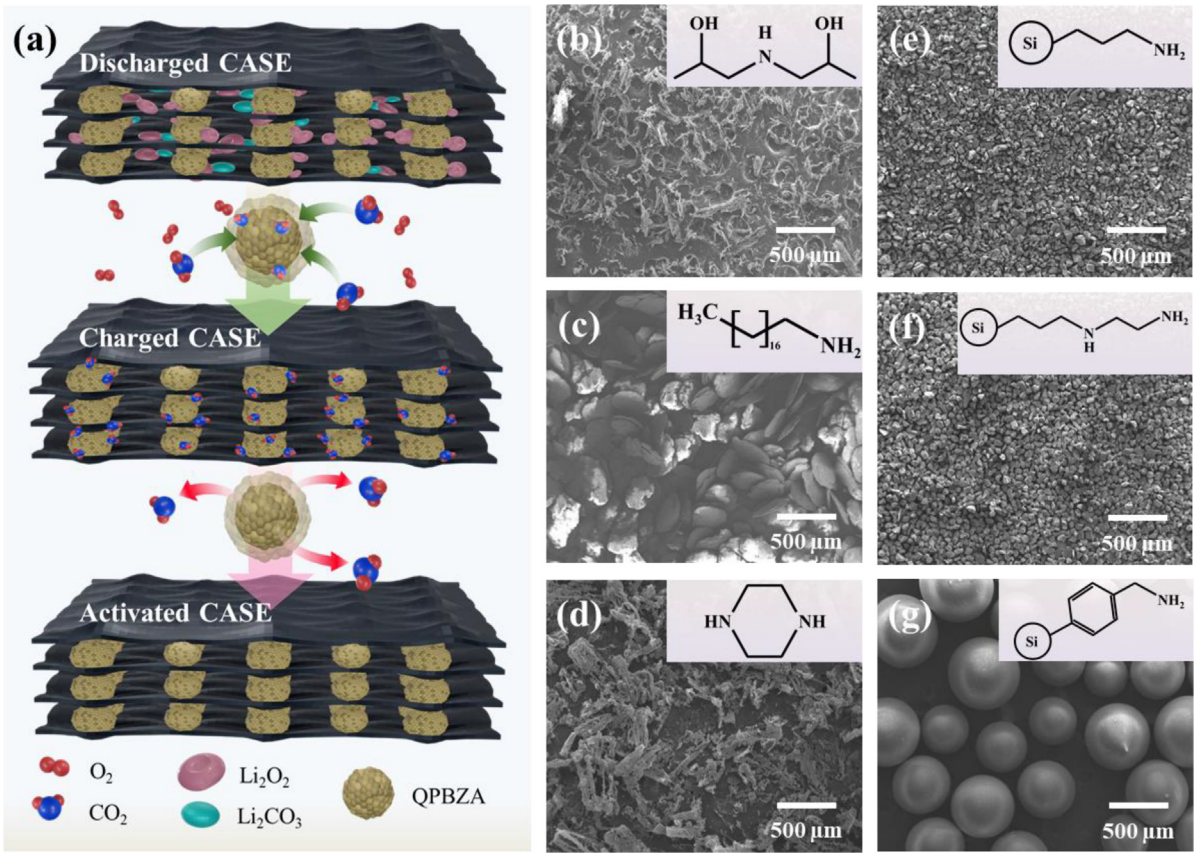

Fig. 2. (a) Schematic illustration of CASE with CAMs for a practical closed Li–O_2 cell. SEM images and chemical structures of CAM candidates with amine group (b) DIPA, (c) ODA, (d) PZ, (e) AP Sg, (f) EDP Sg, and (g) QPBZA.

however, the others appeared to stably maintain their initial state even after 24 h. Each CAM was filtered, and the weight change was recorded to obtain more information on the solubility (Fig. S2). Through this simple solubility test, the highly soluble DIPA and PZ were screened out as candidates for the CAM.

High thermal stability of the CAM for application in a practical cell is another important factor because the CAM is designed to reactivate through a heat-treatment process for reuse. Using differential scanning calorimetry (DSC), the thermal behaviors of the CAMs were investigated from room temperature to 210 °C at a heating rate of 10 °C min^{-1} under N_2 atmosphere. As shown in Fig. 3(b), DIPA, ODA, and PZ underwent phase changes under mild temperature conditions (<120 °C). However, the specific chemical groups functionalized by silica gel (AP Sg, EDP Sg, and QPBZA) did not undergo any distinct temperature-dependent phase transitions until the high temperature of 210 °C as the task-specific functional groups was tightly embedded on the silica gel. From the solubility and thermal stability tests, the three candidates of AP Sg, EDP Sg, and QPBZA were identified as the only applicable CAM candidates.

The most important factor for a CAM as a CO_2-sponging material is how many CO_2 molecules it can adsorb per unit mass. Thus, the CO_2 adsorption abilities for the pre-screened candidates were measured. They were pre-heated in a vacuum oven at 80 °C for 12 h to clean residual gases arising from the air contamination (i.e., pre-activation process) and then exposed to pure CO_2 gas for 12 h at room temperature to force chemical CO_2 attachment with amine groups. A photograph of each process is provided in the Supporting Information (Fig. S3). The adsorption molar ratio was calculated based on the weight changes before and after the CO_2 injection, and the results are summarized in Fig. 3(c). The calculation details are described in the table in Fig. S4. It should be noted that the CO_2 adsorption ability of QPBZA was superior to that of AP Sg and EDP Sg. The percentage of weight changed after the CO_2 adsorption was the greatest for QPBZA (112.41%), as indicated in the normalized bar graphs and described by the line graph of the CO_2 adsorption rate. For the calculation in terms of molecular weight (purple line), 15 molecules of CO_2 could be adsorbed per unit molecule of QPBZA, whereas at most 0.5 and 1 CO_2 molecules could be adsorbed per unit molecule of AP Sg and EDP Sg, respectively. In addition, to verify whether the CAMs could be reactivated, they were simply heat-treated again (i.e., reactivated CAM) at 80 °C for 30 min in a vacuum condition. After the CO_2 desorption processes, the weight of all the candidates decreased, implying that the entangled CO_2 could be thermally detached and that they were simply reusable in Li–O_2 cells. They possessed high CO_2 desorption rates of over 90%, which is expected to further increase when drying under harsh conditions. A summary of our feasibility tests (Fig. S5) indicated that QPBZA is the most suitable candidate for the CAM material.

Before electrode fabrication, the pristine QPBZA was treated to obtain micro-sized particles because small particles would be kinetically advantageous to adsorb CO_2 and be beneficial for forming a robust structure of a self-standing air electrode. Using the ball-milling process, the pristine QPBZA particles with ~ 500 μm diameter (Fig. 2g) were mechanically grinded into micro-sized particles (1–100 μm diameter). SEM images of the pristine QPBZA and treated QPBZA (T-QPBZA) are provided in the Supporting Information (Fig. S6). To investigate the changes in the surface area and pore characteristics of the T-QPBZA, Brunauer-Emmett-Teller (BET) and pore size distributions were analyzed (Fig. 3d and e). Although the surface area slightly decreased from 43.23 to

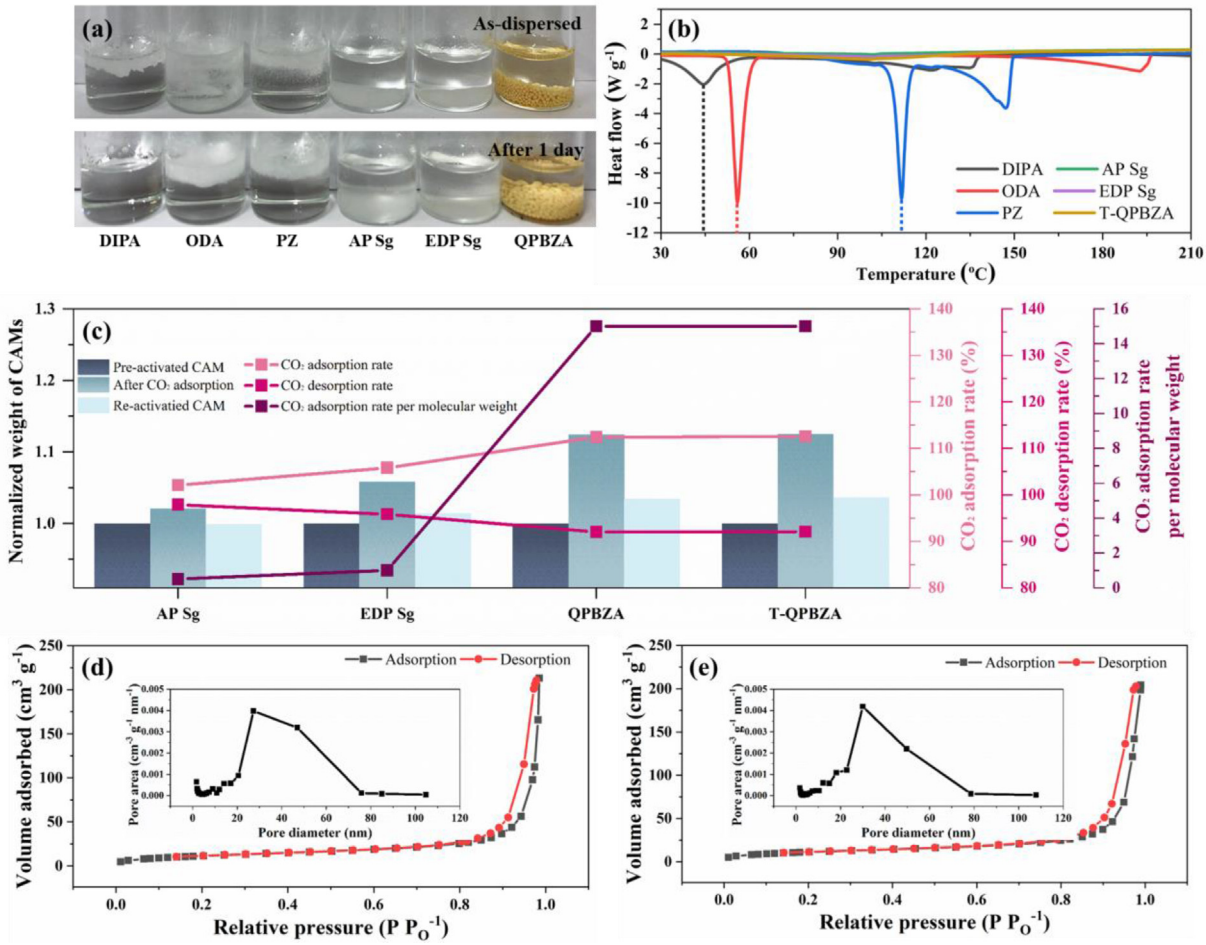

Fig. 3. (a) Solubility test in the electrolyte and (b) DSC analysis for the CAM candidates. (c) CO_2 adsorption and desorption tests for AP Sg, EDP Sg, and QPBZA. BET analyses for (d) QPBZA and (e) T-QPBZA (inset: corresponding pore-size distributions).

41.70 $m^2\ g^{-1}$ after the ball-milling process, their overall pore sizes and distributions remained similar. In brief, the individual particle size of T-QPBZA was successfully reduced through the simple mechanical milling process while its pore characteristics and pore volumes remained unchanged. The high CO_2-adsorption ability of T-QPBZA per unit molecule was comparable to that of QPBZA (Fig. 3c), which proves again that its overall pore structure was well preserved.

To closely investigate whether the CAM material could chemically adsorb CO_2 molecules, binding analysis was performed using Fourier-transform infrared spectroscopy (FT-IR). The pristine AP Sg (Fig. 4a), EDP Sg (Fig. 4b), and QPBZA (Fig. 4c) were heat-treated at 80 °C under vacuum conditions to eliminate residual gases inside. Then, in the pre-activated CAMs, pure CO_2 gas was injected for 12 h for CO_2 adsorption. In the pristine states (black lines), small bonding peaks of N-COO^- and COO^- were observed, corresponding to CO_2 molecules from the ambient air in the pristine particles. The intensity of each peak decreased after the pre-activation step (green lines), implying that the adsorbed CO_2 molecule was well detached [30,31]. Notably, after the CO_2 adsorption process (pink lines), the relevant peaks were clearly dominant again, which indicates that the reversible CO_2 adsorption and desorption could proceed in the selected CAMs. The bonding peaks related to N-COO^- and COO^- after the CO_2 adsorption were more obvious for QPBZA than for AP Sg and EDP Sg, verifying the superior CO_2 adsorption ability of QPBZA, which agrees well with the results of the gas adsorption test (Fig. 3c). X-ray photoelectron spectroscopy (XPS) was additionally used to trace the change in the bonding characteristic affected by the CO_2 adsorption. In the XPS spectra of AP Sg (Fig. 4d), EDP Sg (Fig. 4e), and QPBZA (Fig. 4f), the intensity of the original N–H peak (red line) in the pre-activated process decreased after the CO_2 adsorption. Instead, a newly formed peak corresponding to N–(C = O) binding at 399.2 eV [32] (green region) appeared, offering direct evidence of the CO_2 adsorption reaction by considering the reaction mechanism ($CO_2 + 2RNH_2 \leftrightarrow RNHCOO^- + RNH_3^+$). Notably, the peak intensity was the strongest for the QPBZA, confirming its great CO_2 adsorption ability. The XPS and FT-IR spectra prove that the selected CAMs enable the capture of CO_2 molecules, with QPBZA exhibiting the most outstanding performance.

To apply the selected QPBZA in a practical Li–O_2 cell, the prepared T-QPBZA was mixed with multi-walled carbon nanotubes (MWCNTs) and then fabricated into a CASE. MWCNTs were selected as the substrate carbon because they are relatively resistive to parasitic side reactions and can form a binder-free self-standing electrode [33,34]. The detailed properties of the MWCNTs are described in the Supporting Information (Fig. S7). The amount of T-QPBZA for the CASE should sufficiently receive all $^*CO_2$ evolved during a charge; however, the minimum amount is practically preferred. Therefore, it was necessary to quantify the expected amount of $^*CO_2$ during the first charge. A Li–O_2 cell with bare MWCNTs was discharged to 3 mAh (0.1 mA cm^{-2}), and the amount of Li_2O_2 was measured using the iodometric titration method [35]. This evaluation was repeated three times, and the

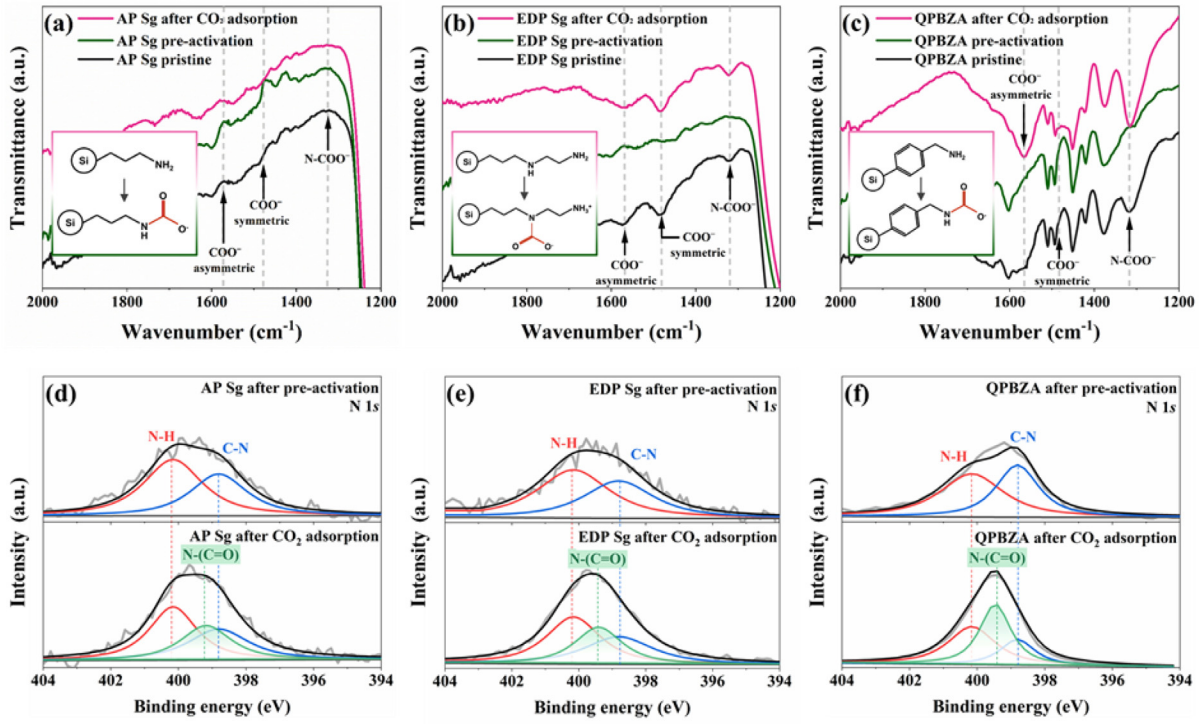

Fig. 4. (a–c) FT-IR analyses for CAMs of AP Sg, EDP Sg, and QPBZA. Each inset shows the reaction mechanism of the CAM candidates with CO_2. (d–f) XPS analyses for N 1 *s* core levels after pre-activation (before CO_2 adsorption) and after CO_2 adsorption.

average yield of Li_2O_2 was calculated to be 64.71% (Fig. 5a). This result implies that the remaining 35.29% can be attributed to side reactions. Under the assumption that all the side reactions are related to the formation of Li_2CO_3, the maximum amount of CO_2 potentially evolved during a charge was calculated to be 19.59 μmol. To directly measure the CO_2 gas evolved during a charge, quantitative analysis using DEMS was performed (Fig. 5b). A Li–O_2 cell discharged under the same condition was prepared, and the evolved gas during a charge was flowed into the DEMS system. The total amount of released O_2 was 42.16 μmol, corresponding to 64.51% of the Li_2O_2 yield, which is similar to the value measured using the titration method in Fig. 5(a). In contrast,

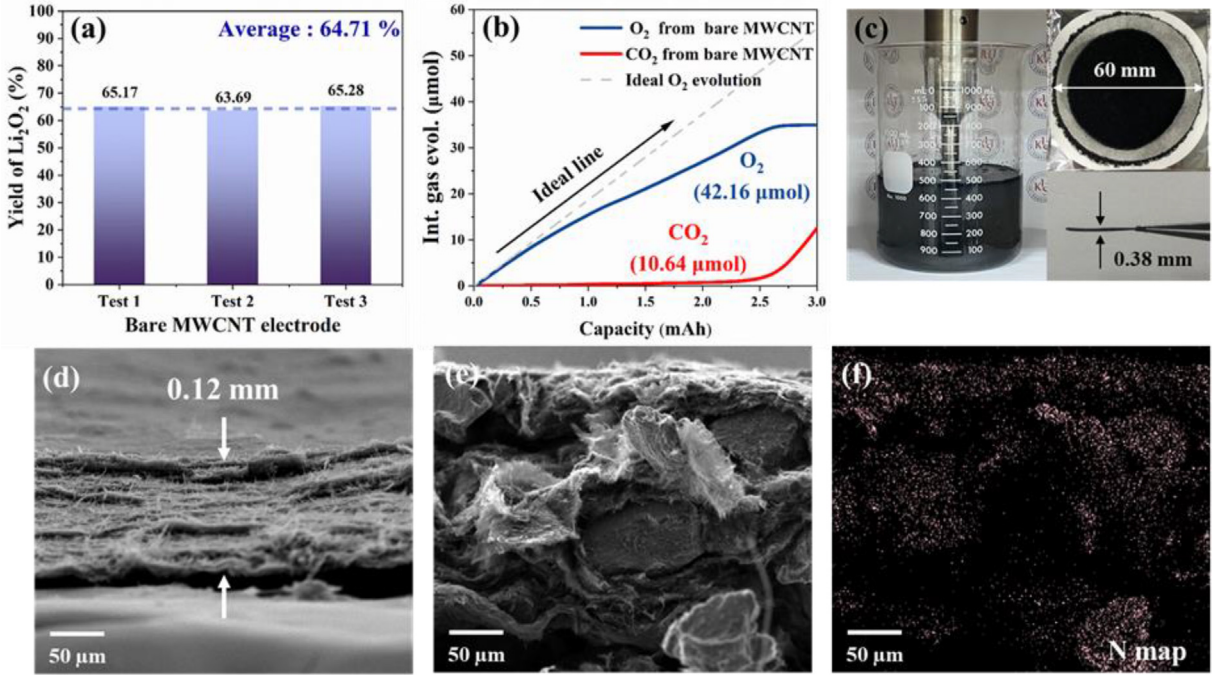

Fig. 5. (a) Average yield of Li_2O_2 discharge product for the three different Li–O_2 cells determined by iodometric titration. (b) DEMS quantitative analysis of Li–O_2 cell with bare MWCNT electrode on charge. (c) Images of fabricated binder-free self-standing CASE. SEM images of cross section of (d) bare MWCNT with 0.12-mm thickness and (e) CASE with 0.38-mm thickness. (f) EDS mapping image corresponding to CASE in (e).

almost half of the CO_2 (10.64 μmol) compared with the expected volume (19.59 μmol) was detected. Considering both the CO_2 adsorption rate and the detected CO_2 volume, the minimum amount of T-QPBZA was calculated (Fig. S8).

A slurry of CASE was prepared by mixing the MWCNTs and T-QPBZA without any binder in acetone and distilled water solution. After vigorous tip sonication, the slurry was filtrated and dried, forming a self-standing CASE (Fig. 5c). The slurry-based synthesis is advantageous for mass production (e.g., 60 mm diameter in our case, inset of Fig. 5c) as the size of the filter or substrate can be easily adjusted. Through filtration of the slurry, a film-like MWCNT electrode can be formed and configured into numerous stacked layers. When T-QPBZA was not included, the thickness of the bare MWCNT electrode was approximately 0.12 mm (Fig. 5d). It should be mentioned that the T-QPBZA also plays an important role as a mechanical buffer; the micro-sized particles placed between the stacked MWCNT layers contribute to the formation a porous structure. As a result, a thicker CASE with an average thickness of 0.38 mm (inset of Fig. 5c) was obtained. The cross-sectional SEM image (Fig. 5e) and corresponding energy-dispersive X-ray spectroscopy (EDS) mapping image (Fig. 5f) show the increased porosity of the CASE compared with that of the bare MWCNT electrode, and the T-QPBZA particles are observed to be well distributed (Fig. S9). This unique feature was expected to allow fast breathing of gaseous products including O_2, CO_2, and $^*CO_2$ and help to improve the wettability with the electrolyte. This advantage was confirmed by comparing the discharge capacities after fully discharging to 2.0 V (Fig. S10). The porous CASE buffered by T-QPBZA particles delivered a much higher discharge capacity of approximately 25 mAh cm^{-2} compared with that of the bare MWCNT electrode (~10 mAh cm^{-2}). Furthermore, EIS analysis confirmed that the unique structure of the CASE improved wettability to the electrolyte, resulting in lower resistance than the MWCNT electrode (Fig. S11).

The prepared CASE was electrochemically cycled, and its effect on eliminating CO_2 was investigated. To verify whether T-QPBZA was electrochemically stable in the voltage range between 2.0 and 4.5 V, cyclic voltammetry (CV) tests were performed under Argon atmosphere, as shown in Fig. 6(a). The results demonstrate that T-QPBZA was stable under 4.5 V, and the oxidations over 4.5 V were attributed to the electrolyte decompositions. The CV results under O_2 atmosphere (inset of Fig. 6a) also prove that the effect of T-QPBZA was electrochemically negligible and that it did not affect the Li_2O_2 reaction. To examine the effect of T-QPBZA as a CO_2-sponging agent, Li–O_2 cells with the bare MWCNT electrode and the CASE were compared. Each was pre-discharged to 3 mAh, and the evolved gas during a charge was analyzed using DEMS. For the bare MWCNT electrode (Fig. 6b), although only O_2 was evolved in the initial charge ranges, a large amount of CO_2 was detected at high voltages over 4.0 V. Notably, for the cell with the CASE, CO_2 was not released at all in the entire voltage region thanks to the effect of T-QPBZA (Fig. 6c). The comparison graph for the evolved gases (Fig. 6d) shows the clear difference in the CO_2 evolution, especially near the high-voltage areas. However, the released O_2 amounts were similar: 38.40 μmol for the bare MWCNT electrode and 37.97 μmol for the CASE, indicating the selective CO_2 adsorption ability of T-QPBZA. It was demonstrated that the CASE effectively eliminated the evolved CO_2 during a charge; therefore, we supposed that the undesirable CO_2 incorporation in a successive discharge might be prevented. To investigate the effect of the CASE on the reaction route, a second discharge was analyzed using the GITT technique (Fig. 6e). The equilibrium potential of the bare MWCNT electrode at the second discharge relaxed close to 3.18 V, which is higher than the theoretical Li_2O_2 formation voltage (2.96 V). The high equilibrium potential is attributed to the CO_2 incorporation as well as the formation of Li_2CO_3, which are the major contributors to cycle degradation [14,36]. Interestingly, the cell with the CASE possessed a relatively lower equilibrium potential, indicating greater proceeding of the ideal Li_2O_2 reaction, which is attributed to the restricted $^*CO_2$ incorporation. It is further proved by EIS test in Fig. S11. This result indicates that the CASE was able to adsorb CO_2 in a practical Li–O_2 cell; thus, it could change the reaction route to the ideal reaction path by preventing the CO_2 incorporation. As a result, the CASE improved the cyclabil-

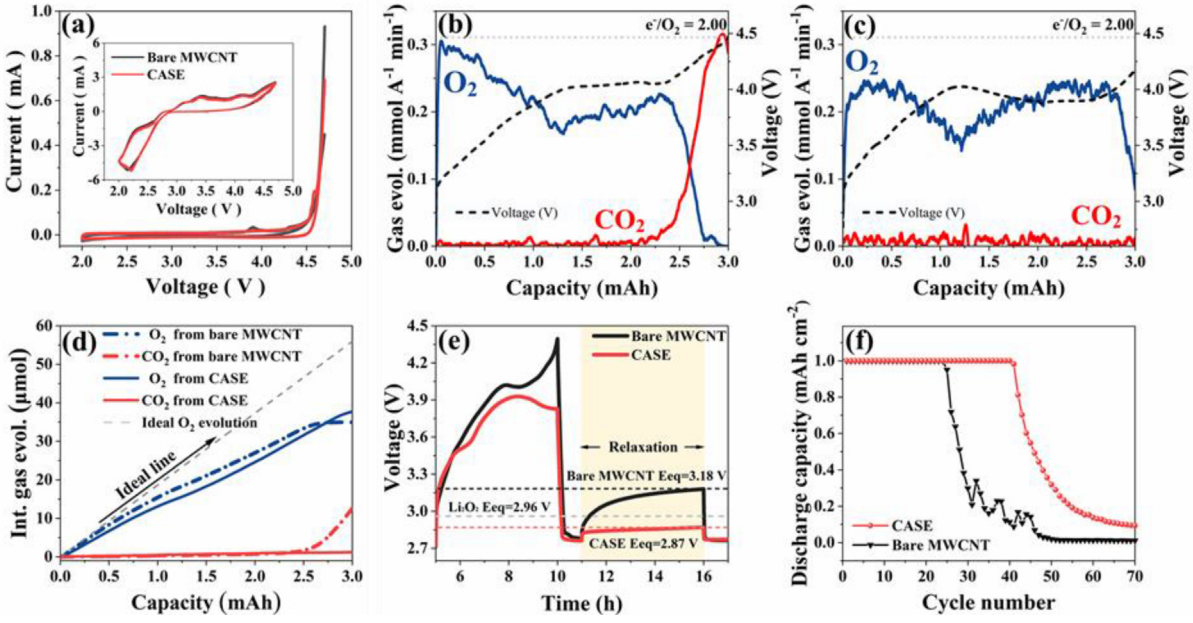

Fig. 6. (a) Cyclic voltammetry tests for bare MWCNT electrode and CASE under argon atmosphere (inset: under O_2 atmosphere). DEMS analysis on first charge with (b) bare MWCNT electrode and (c) CASE. (d) Comparison of O_2 and CO_2 gases generated from two different electrodes. (e) Galvanostatic intermittent titration technique (GITT) analysis voltage profile of Li–O_2 cells with bare MWCNT electrode (black line) and CASE (red line) for second discharging with 5 h rest time. (f) Comparison of cycle performance between bare MWCNT electrode (black line) and CASE (red line).

ity of the Li–O_2 cell compared with the bare electrode, as illustrated in Fig. 6(f). In the current state of Li–O_2 batteries, parasitic reactions, especially from the reactive oxygen radicals, cannot be perfectly prevented; however, the approach of applying a CAM may provide a new path to practically advance Li–O_2 batteries.

4. Conclusions

To regulate the CO_2-incorporation reaction in Li–O_2 batteries, a new electrode architecture decorated with CO_2-spongy material is first demonstrated. To identify the most appropriate CO_2-adsorbent material, various amine-functionalized task-specific candidates were screened, and QPBZA was selected owing to its high gas adsorption capability per unit molecule. Through gas adsorption tests, QPBZA was demonstrated to effectively and selectively adsorb CO_2 (15 molecules of CO_2 per unit molecule). A CO_2-adsorbent spongy electrode was prepared by decorating micro-sized QPBZA particles sandwiched between porous carbon sheets. The unique porous structure attributed to the micro-sized QPBZA particles in the layered scaffold is advantageous as it provides fast transfer pathways for reactants and can markedly suppress the evolution of CO_2 during a charge process. The novel electrode architecture with CO_2-adsorbent spongy material helped alter the reaction pathways from the formation of Li_2CO_3 to the ideal Li_2O_2 reaction by suppressing the $^*CO_2$ incorporation reaction. As a result, the evolution of CO_2 during a charge was prevented, leading to reduced Li_2CO_3 formation as well as increased cyclability. These findings will contribute to opening a new path for the realization of practical Li–O_2 batteries.

Declaration of Competing Interest

The authors declare that they have no known competing financial interests or personal relationships that could have appeared to influence the work reported in this paper.

Acknowledgments

This work was supported by the National Research Foundation of Korea(NRF) grant funded by the Korea government(MSIT) (No. 2021R1C1C1003628), the Development Program of Core Industrial Technology, funded by the Ministry of Trade, Industry & Energy of Korea (20012318), and the institutional program of the Korea Institute of Science and Technology (2E31001).

Appendix A. Supplementary data

Supplementary data to this article can be found online at https://doi.org/10.1016/j.jechem.2021.06.022.

References

[1] P.G. Bruce, S.A. Freunberger, L.J. Hardwick, J.-M. Tarascon, Nat. Mater. 11 (2012) 19–29.
[2] N. Feng, P. He, H. Zhou, Adv. Energy Mater. 6 (2016) 1502303.
[3] K. Abraham, Z. Jiang, J. Electrochem. Soc. 143 (1996) 1–5.
[4] J. Kang, J.M. Kim, D.Y. Kim, J. Suk, J. Kim, D.W. Kim, Y. Kang, J. Energy Chem. 48 (2020) 7–13.
[5] H. Xia, Q. Xie, Y. Tian, Q. Chen, M. Wen, J. Zhang, Y. Wang, Y. Tang, S. Zhang, Nano Energy 84 (2021) 105877.
[6] X. Hu, G. Luo, Q. Zhao, D. Wu, T. Yang, J. Wen, R. Wang, C. Xu, N. Hu, J. Am. Chem. Soc. 142 (2020) 16776–16786.
[7] M. Armand, J.-M. Tarascon, Nature 451 (2008) 652–657.
[8] A.C. Luntz, B.D. McCloskey, Chem. Rev. 114 (2014) 11721–11750.
[9] F. Li, T. Zhang, H. Zhou, Energy Environ. Sci. 6 (2013) 1125–1141.
[10] J. Lu, L. Li, J.-B. Park, Y.-K. Sun, F. Wu, K. Amine, Chem. Rev. 114 (2014) 5611–5640.
[11] S.A. Freunberger, Y. Chen, Z. Peng, J.M. Griffin, L.J. Hardwick, F. Bardé, P. Novák, P.G. Bruce, J. Am. Chem. Soc. 133 (2011) 8040–8047.
[12] M.M. Ottakam Thotiyl, S.A. Freunberger, Z. Peng, P.G. Bruce, J. Am. Chem. Soc. 135 (2013) 494–500.
[13] Z. Zhao, J. Huang, Z. Peng, Angew. Chem. Int. Ed. 57 (2018) 3874–3886.
[14] H.-K. Lim, H.-D. Lim, K.-Y. Park, D.-H. Seo, H. Gwon, J. Hong, W.A. Goddard, H. Kim, K. Kang, J. Am. Chem. Soc. 135 (2013) 9733–9742.
[15] J.L. Roberts Jr, T.S. Calderwood, D.T. Sawyer, J. Am. Chem. Soc. 106 (1984) 4667–4670.
[16] N. Mahne, S.E. Renfrew, B.D. McCloskey, S.A. Freunberger, Angew. Chem. Int. Ed. 57 (2018) 5529–5533.
[17] S. Yang, P. He, H. Zhou, Energy Environ. Sci. 9 (2016) 1650–1654.
[18] B. McCloskey, A. Speidel, R. Scheffler, D. Miller, V. Viswanathan, J. Hummelshøj, J. Nørskov, A. Luntz, J. Phys. Chem. Lett. 3 (2012) 997–1001.
[19] B.M. Gallant, R.R. Mitchell, D.G. Kwabi, J. Zhou, L. Zuin, C.V. Thompson, Y. Shao-Horn, J. Phys. Chem. C 116 (2012) 20800–20805.
[20] J. Kang, J. Kim, S. Lee, S. Wi, C. Kim, S. Hyun, S. Nam, Y. Park, B. Park, Adv. Energy Mater. 7 (2017) 1700814.
[21] M.M. Ottakam Thotiyl, S.A. Freunberger, Z. Peng, Y. Chen, Z. Liu, P.G. Bruce, Nat. Mater. 12 (2013) 1050–1056.
[22] D. Cao, S. Zhang, F. Yu, Y. Wu, Y. Chen, Batteries Supercaps 2 (2019) 428–439.
[23] W.-J. Kwak, H. Kim, Y.K. Petit, C. Leypold, T.T. Nguyen, N. Mahne, P. Redfern, L. A. Curtiss, H.-G. Jung, S.M. Borisov, Nat. Commun. 10 (2019) 1–8.
[24] S. Ma, Y. Wu, J. Wang, Y. Zhang, Y. Zhang, X. Yan, Y. Wei, P. Liu, J. Wang, K. Jiang, Nano Lett. 15 (2015) 8084–8090.
[25] K. Takechi, T. Shiga, T. Asaoka, Chem. Commun. 47 (2011) 3463–3465.
[26] J.-H. Kang, J. Lee, J.-W. Jung, J. Park, T. Jang, H.-S. Kim, J.-S. Nam, H. Lim, K.R. Yoon, W.-H. Ryu, ACS nano 14 (2020) 14549–14578.
[27] S.R. Gowda, A. Brunet, G.M. Wallraff, B.D. McCloskey, J. Phys. Chem. Lett. 4 (2013) 276–279.
[28] R. Serna-Guerrero, E. Da'na, A. Sayari, Ind. Eng. Chem. Res. 47 (2008) 9406-9412.
[29] S. Choi, M.L. Gray, C.W. Jones, ChemSusChem 4 (2011) 628–635.
[30] G. Richner, Energy Procedia 37 (2013) 423–430.
[31] Ernoe Pretsch, Philippe Bühlmann, Christian Affolter (Eds.), Structure Determination of Organic Compounds, Springer Berlin Heidelberg, Berlin, Heidelberg, 2000.
[32] Y. Hai, J. Zhang, C. Shi, A. Zhou, C. Bian, W. Li, J. Membr. Sci. 520 (2016) 19–28.
[33] H.D. Lim, K.Y. Park, H. Song, E.Y. Jang, H. Gwon, J. Kim, Y.H. Kim, M.D. Lima, R.O. Robles, X. Lepró, Adv. Mater. 25 (2013) 1348–1352.
[34] H.-D. Lim, Y.S. Yun, S.Y. Cho, K.-Y. Park, M.Y. Song, H.-J. Jin, K. Kang, Carbon 114 (2017) 311–316.
[35] B.D. McCloskey, A. Valery, A.C. Luntz, S.R. Gowda, G.M. Wallraff, J.M. Garcia, T. Mori, L.E. Krupp, J. Phys. Chem. Lett. 4 (2013) 2989–2993.
[36] Z.H. Cui, X.X. Guo, H. Li, Energy Environ. Sci. 8 (2015) 182–187.